Observations of artefacts in the x-ray ptychography method

Nicolas Burdet[1], Graeme R. Morrison[1], Xiaojing Huang[2], Xiaowen Shi[1], Jesse N. Clark[1], Fucai Zhang[1], Maria Civita[1], Ross Harder[3] and Ian K. Robinson[1]

[1]*London Centre for Nanotechnology, University College London, London WC1H 0AH, UK and Research Complex at Harwell, Harwell Campus, Oxford, OX11 0QF, UK,*

[2]*National Synchrotron Light Source II, Brookhaven National Laboratory, Upton, New York 11973, USA.*

[3]*Advanced Photon Source, Argonne, Illinois 60439, USA.*

nicolas.burdet.10@ucl.ac.uk

Abstract:
X-ray ptychography, a scanning coherent diffraction imaging method, was used to reconstruct images of a "Siemens star" test pattern with amplitude and phase contrast. While studying how the use of illumination with an increased bandwidth results in clear improvements in the quality of image reconstructions, we found that an artificial change in the overall distance scale factor of the algorithm leads to a systematic response in the image, which is reproduced with an incorrect number of spokes. This pathology is explained by the conflict between the length scales set by the scan and by the diffraction patterns on the detector.

OCIS codes: (100.5070) Phase retrieval; (170.3010) Image reconstruction techniques; (340.7440) X-ray imaging

References and links

1. J. R. Fienup, "Phase retrieval algorithms - a comparison," Appl. Opt. **21**, 2758–2769 (1982).
2. J. M. Rodenburg and H. M. L. Faulkner, "A phase retrieval algorithm for shifting illumination," Appl. Phys. Lett. **85**, 4795–4797 (2004).
3. P. Thibault, M. Dierolf, O. Bunk, A. Menzel, and F. Pfeiffer, "Probe retrieval in ptychographic coherent diffractive imaging," Ultramicroscopy **109**, 338–343 (2009).
4. A. M. Maiden and J. M. Rodenburg, "An improved ptychographical phase retrieval algorithm for diffractive imaging," Ultramicroscopy **109**, 1256–1262 (2009).
5. P. Thibault and A. Menzel, "Reconstructing state mixtures from diffraction measurements," Nature **494**, 68–71 (2013).
6. F. Zhang, I. Peterson, J. Vila-Comamala, A. D. F. Berenguer, R. Bean, B. Chen, A. Menzel, I. K. Robinson, and J. M. Rodenburg, "Translation position determination in ptychographic coherent diffraction imaging," Opt. Express **21**, 13592–13606 (2013).
7. J. N. Clark, C. T. Putkunz, E. K. Curwood, D. J. Vine, R. Scholten, I. McNulty, K. A. Nugent, and A. G. Peele, "Dynamic sample imaging in coherent diffractive imaging," Opt. Lett. **36**, 1954–1956 (2011).
8. L. W. Whitehead, G. J. Williams, H. M. Quiney, D. J. Vine, R. A. Dilanian, S. Flewett, K. A. Nugent, A. G. Peele, E. Balaur, and I. McNulty, "Diffractive imaging using partially coherent x rays," Phys. Rev. Lett. **103**, 243902 (2009).
9. J. N. Clark, G. J. Williams, H. M. Quiney, L. Whitehead, M. D. de Jonge, E. Hanssen, M. Altissimo, K. A. Nugent, and A. G. Peele, "Quantitative phase measurement in coherent diffraction imaging," Opt. Express **16**, 3342–3348 (2008).

10. P. Godard, M. Allain, and V. Chamard, "Imaging of highly inhomogeneous strain field in nanocrystals using x-ray Bragg ptychography: A numerical study," Phys. Rev. B **84**, 144109 (2011).
11. M. Dierolf, A. Menzel, P. Thibault, P. Schneider, C. M. Kewish, R. Wepf, O. Bunk, and F. Pfeiffer, "Ptychographic x-ray computed tomography at the nanoscale," Nature **467**, 436–439 (2010).
12. B. Chen, M. Guizar-Sicairos, G. Xiong, L. Shemilt, A. Diaz, J. Nutter, N. Burdet, S. Huo, J. Mancuso, A. Monteith, F. Vergeer, A. Burgess, and I. Robinson, "Three-dimensional structure analysis and percolation properties of a barrier marine coating," Sci. Rep. **3**, 1177 (2013).
13. P. Thibault, M. Dierolf, O. Bunk, A. Menzel, and F. Pfeiffer, "Probe retrieval in ptychographic coherent diffractive imaging," Ultramicroscopy **109**, 338–343 (2009).
14. M. Guizar-Sicairos, M. Holler, A. Diaz, J. Vila-Comamala, O. Bunk, and A. Menzel, "Role of the illumination spatial-frequency spectrum for ptychography," Phys. Rev. B **86**, 100103 (2012).
15. A. Fannjiang and W. Liao, "Phase retrieval with random phase illumination," J. Opt. Soc. Am. A **29**, 1847–1859 (2012).
16. A. Oppenheim, M. Hayes, and J. Lim, "Iterative procedures for signal reconstruction from fourier-transform phase," Opt. Eng. **21**, 122–127 (1982).
17. ZonePlates Ltd, 8 South Way, Claverings Industrial Estate, London N9 OAB, UK, URL http://www.zoneplates.com. .
18. M. Dierolf, P. Thibault, A. Menzel, C. M. Kewish, K. Jefimovs, I. Schlichting, K. von König, O. Bunk, and F. Pfeiffer, "Ptychographic coherent diffractive imaging of weakly scattering specimens," New J. Phys. **12** 035017 (2010).
19. O. Bunk, M. Dierolf, S. Kynde, I. Johnson, O. Marti, and F. Pfeiffer, "Influence of the overlap parameter on the convergence of the ptychographical iterative engine," Ultramicroscopy **108**, 481–487 (2008).
20. X. Huang, M. Wojcik, N. Burdet, I. Peterson, G. R. Morrison, D. J. Vine, D. Legnini, R. Harder, Y. S. Chu, and I. K. Robinson, "Quantitative x-ray wavefront measurements of Fresnel zone plate and k-b mirrors using phase retrieval," Opt. Express **20**, 24038–24048 (2012).
21. H. F. Talbot, "LXXVI. Facts relating to optical science. No. IV," Phil. Mag. Ser. 3 **9**, 401–407 (1836).
22. F. J. Salgado-Remacha, L. M. Sanchez-Brea, and E. Bernabeu, "Effect of fill-factor on the Talbot effect of diffraction gratings," J. Europ. Opt. Soc. Rap. Public. **6**, 11055 (2011).
23. J. N. Clark, X. Huang, R. Harder, and I. K. Robinson, "High-resolution three-dimensional partially coherent diffraction imaging," Nat. Commun. **3**, 993 (2012).

1. Introduction

Coherent Diffraction Imaging (CDI) is a rapidly developing tool of optics. Its main advantage is the ability to obtain images from the diffraction patterns alone, without the need for lenses [1]. It makes use of phase retrieval techniques to allow the computation of the image as a simple Fourier transform of its complex diffraction pattern. Ptychography involves shifting the probe in small steps to record diffraction patterns from overlapping regions, and the introduction of a real-space overlap constraint made the reconstruction methods more robust by providing additional redundancy in the information given by the measurements [2]. This extra information allows complete characterisation of the complex sample transmission function and the scanned illumination wavefield, called the "probe" [3, 4], through recovery of their respective modes [5]. It also allows retrieval of their relative positions in real-space [6], providing ways of dealing with experimental problems such as vibrations [7], partial coherence [8] and uncertainties in scan positions. Both single-shot CDI and ptychography produce phase contrast in the image of the object, and can achieve high accuracy in the phase measurement [9]. Ptychography also alleviates some of the problems with single-measurement CDI methods, such as convergence difficulties for strong phase objects [10], and has proved to be a quantitative and non-destructive microscopy technique for two- and three-dimensional images that is successful for nano-materials and biological objects [11, 12].

In the infancy of ptychography, the illumination profile formed by a lens or other optical component had to be simulated or known [2]. Now that reconstructions are readily obtainable using improved algorithms [4, 13] that require only rough initial estimates of the probe, the resolution [14] and convergence of the reconstructions [15] are subjects of continuing interest. In CDI, non-uniqueness was declared to be pathologically rare for the 2D and 3D cases [16]. The redundancy in ptychography should in principle prevent non-uniqueness artefacts but this

is not yet established. There are simple symmetry concerns which can affect the reliability of reconstructions of phase structures when the probe structure is unknown. For example, the zero-order and linear components of the probe and object phase structures can cancel each other. It is therefore acceptable to remove arbitrary phase ramps which appear in an image reconstruction.

In the experiments reported here, we investigated the behaviour of ptychographic algorithms using "Siemens star" test objects, and explored the effect of the probe bandwidth on the quality of the reconstructions obtained. In the course of these studies, we found that artefacts are present in the reconstructed images when the overall distance scale factor is not accurately known.

2. Experimental set-up

Experiments were carried out at beamline 34-ID-C at the Argonne National Laboratory. The experimental set-up in the forward-scattering geometry is presented in schematic form in Fig. 1(a).

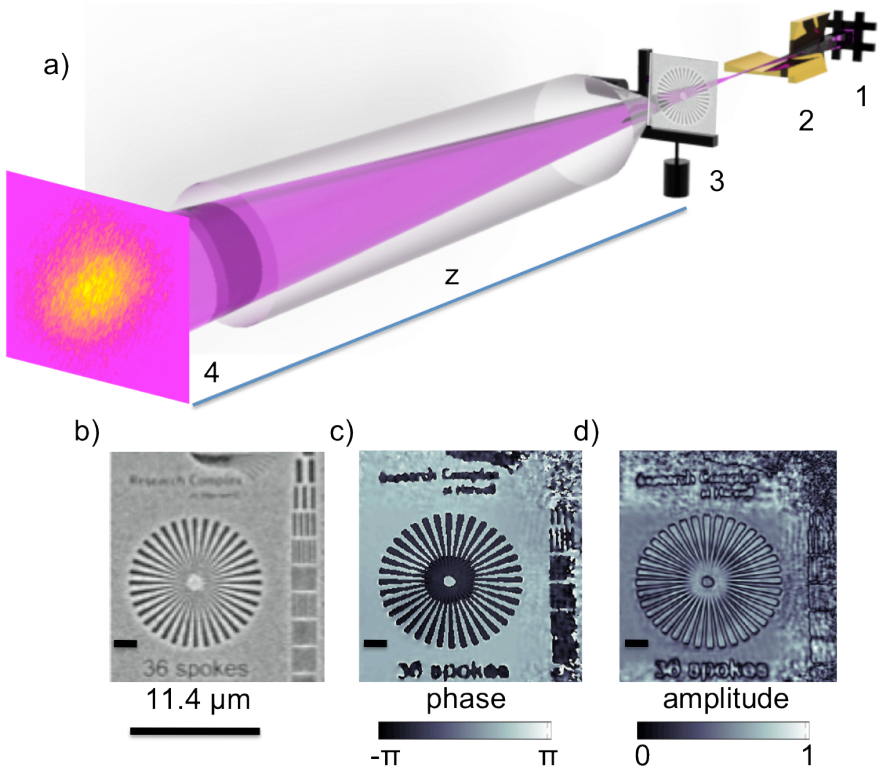

Fig. 1. (a) Sketch of the experimental setup at 34-ID-C with entrance slits (1), KB mirrors (2), piezo-stage (3) and camera (4). A flight tube represented as a semi-transparent tube here is used only for distances above 1 m. (b) SEM image of the test pattern. Siemens star, diameter 11.4 μm. (c),(d) show reconstructed phase and amplitude images using data measured at z =2.184 m. Scale bars inside images, 2 μm.

The X-ray probe was generated by means of a Kirkpatrick-Baez (KB) mirror system and its size was varied by changing the size of the entrance pupil. The customized test pattern (shown in Fig. 1(b)) is used during the initial stage of our experiments at APS to assist in the successful recovery of both amplitude and phase of more general objects. It was fabricated to our specification by ZonePlates Ltd [17] using electron beam lithography and reactive ion

etching. The pattern was prepared in 1.5 μm thick tungsten film evaporated on to a 1 μm thick silicon nitride window, to provide about 70 % intensity transmission and about 0.9π phase shift when illuminated by a 9 keV ($\lambda = 0.138$ nm) X-ray beam. The beam was focused by the KB mirror system placed directly downstream of the coherence-defining slits (which were were adjusted to select the coherent part of the incident beam). The X-ray beam energy was selected by a Si(111) double crystal monochromator, and provided sufficient longitudinal (temporal) coherence for this experiment.

The sample was scanned using an nPoint NPXY100Z25A dual-axis piezo stage, which was mounted on top of a set of XYZ stepper-motors for larger range movements. A Princeton Instrument PI-MTE 1300B charge-coupled device (CCD) with $N \times N$ square pixels of width $\Delta p = 20\,\mu$m was placed downstream at a distance z from the test sample. In the small angle geometry, a Fourier-space pixel of size Δp on the detector is related to a real-space pixel size Δx in the reconstructed image by the formula

$$\Delta x = \frac{\lambda z}{N \Delta p}. \tag{1}$$

In the remainder of the paper, the distance $N\Delta x$ will be referred to as the CDI window, since it corresponds to the interval that could be reconstructed by Fourier transform of a single diffraction pattern.

3. Probe bandwidth experiment

In our set-up, a smaller probe with an increased bandwidth within the CDI window is easily obtained by opening the KB entrance slits wider. According to classical diffraction theory of lenses, the size of the focus scales as the reciprocal of the entrance aperture: ($d \sim 2\lambda f/a$) where d is the focus spot size, f the focal length and a the entrance aperture size. The X-ray beam is effectively coherent within a nominal area of $\sim 30 \times 50\,\mu$m, so it is detrimental to open the slits wider.

To study the effect of probe bandwidth with a significant change between probes within the CDI window, two entrance slit settings that provide full coherence (10×10 μm and 30×50 μm) along with three distances ($z = 0.55$, 1.0 and 2.184 m) which are representative of the available range of camera lengths were chosen. A concentric circular scan trajectory [18] with $5n$ points on the n^{th} ring, and a radius increment dr of $0.5\,\mu$m within a $12 \times 12\,\mu$m scan range, generated 460 frames of far-field diffraction patterns for each measurement. The detector region-of-interest (ROI) was set to $N = 256$ pixels, which gave real-space pixel sizes of $\Delta x = 14$, 24 and 55 nm, respectively, for the three detector distances used. As the focal lengths of the KB mirrors are 100 mm and 200 mm in the horizontal and vertical directions respectively, the two slit settings gave nominal focus sizes of $2.7 \times 5.4\,\mu$m and $0.9 \times 1\,\mu$m.

A reconstruction algorithm based on the difference map (DM) approach [3] was used to retrieve the complex sample and illumination functions from the measured diffraction data. As initial input for the algorithm, a random guess of the sample image and a $1 \times 1\,\mu$m square aperture for the illumination probe were used. For the first 10 iterations, only the object was updated, while the illumination function started to update after 10 iterations until the final number of 100 iterations.

In Fig. 2, we can clearly observe that, for a given distance, sharper edges and improved contrast are given by reconstructions with the smaller probe that has a larger bandwidth. We observe as well that, for longer distances, the "36 spokes" label written on the sample becomes visible beside the star pattern. To explain these results, we can define a quality criterion Ω by coupling into a single product two fundamental quantities of ptychography, the overlap (Θ) and the sampling S as both are varying in this experiment. The overlap is given by $\Theta = (d - dr)/d$,

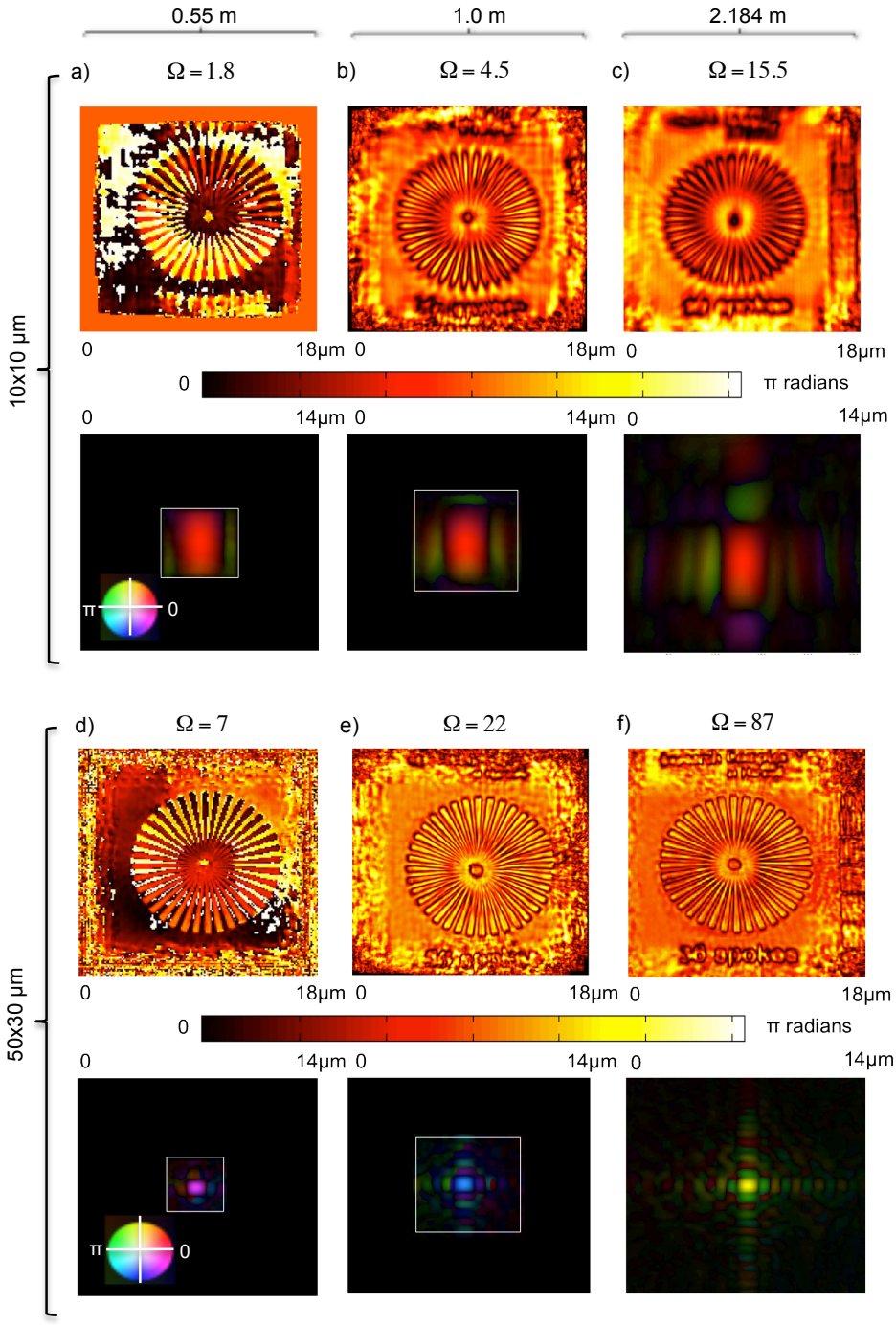

Fig. 2. From left to right: reconstructed objects and probes for detectors located at distance $z = 0.55$, 1.0 and 2.184 m from the sample. Top half: reconstructions for slit openings of $10 \times 10\,\mu$m. Lower half: reconstructions for slit openings of $30 \times 50\,\mu$m (note: the horizontal KB mirror has one half the focal length of the vertical). The probes are shown on a common array scale but a white frame has been drawn to represent the original size of the CDI window. The amplitude of each probe is mapped to the image brightness, and the phase is mapped to hue. The probe sizes are in good agreement with values predicted from diffraction theory.

and the sampling S is defined as the CDI window size divided by the spot size d. The quantity $\Omega = \Theta S$ is an aggregate measure of the over-determination of the phase problem. In principle, the value of Ω for a 1-dimensional calculation should be ≥ 1 as the overlap $\Theta \geq 0.5$ [19] and the sampling $S \geq 2$ to satisfy the Nyquist condition. For 2-dimensional calculations, $S \geq 4$ and the overlap becomes $\Theta = \Theta_x \Theta_y$ (using subscripts x and y for the two lateral dimensions of the probe). From the values that are reported in Fig. 2, it seems that Ω needs to be about an order of magnitude higher than the threshold values given here to obtain good reconstructions.

4. Non uniqueness artefacts

We also investigated the consequences of a 10% uncertainty in the assumed sample-to-camera distance when reconstructing the data measured at distance $z_0 = 0.55\,\mathrm{m}$, and found images with unexpected numbers of spokes appearing.

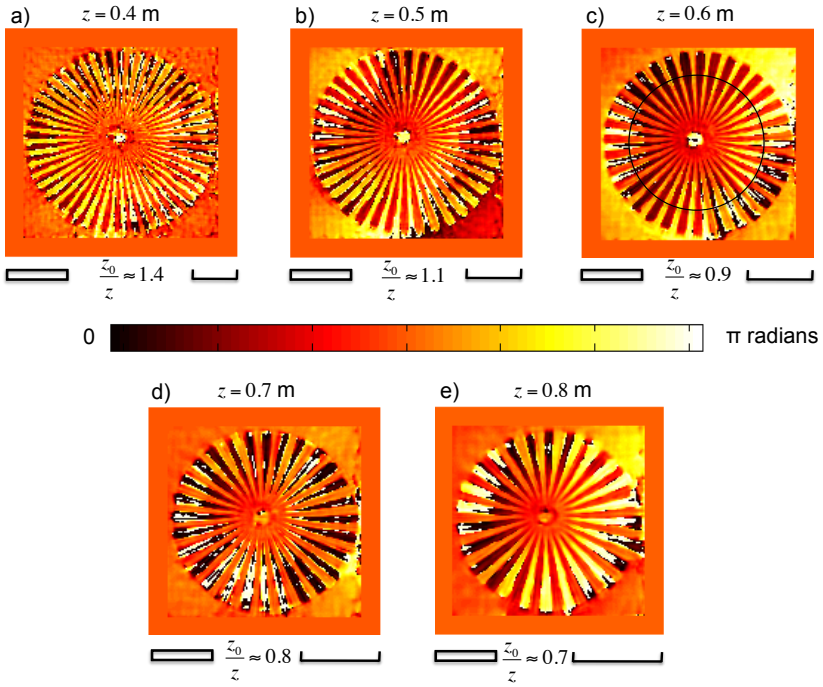

Fig. 3. Reconstructed image phases (a)-(e) for different assumed distances z between sample and detector. The reconstructed object phase at the correct distance z_0=0.55 m are shown in Fig. 2(d). The closed bars (3 μm) are the size of the object set by the piezo scanner, while the open bars are the length scale set by the CDI window size. Their sizes are equal when the distance $z = z_0 = 0.55\,\mathrm{m}$. A circular cut (see Fig. 3(c)) located 3 μm from the centre of each image was used to count the spokes in each reconstruction.

The assumed values for z were allowed to range from $z = 0.4\,\mathrm{m}$ to $z = 0.8\,\mathrm{m}$, and this produced a continuous decrease in spoke numbers as z increased. The methodology for the data collection and the ptychographic reconstructions was the same as described in section 3. There were 17 reconstructions at different z values in the range of interest. It was found that 100 iterations were enough for all the reconstructions to reach a plateau in the error metric. The reconstructed images using incorrect detector-to-sample distances all look plausible reconstructions, in terms of their circular symmetry and the recovered phase values. They also give the

correct diameter of 11.4 μm. The retrieved probes all look very similar (and closely resemble the previously characterised wave-front for the same experimental set-up [20]), and have the same extent in pixels. The relationship between the spoke numbers and the reciprocal of the assumed detector distance z is linear (see Fig. 4), although some small flat regions at discrete integer values of the spoke count can be seen on the plot.

In CDI, the reliability of the reconstructions is monitored by the R-factor [13] which quantifies the agreement with the measured data and computed as

$$R = \frac{\sum_j^J \sum_q^Q (||I_{obs}^j(q)| - |I_{calc}^j(q)||)}{\sum_j^J \sum_q^Q |I_{obs}^j(q)|} \tag{2}$$

(the summation is over the reciprocal-space coordinate q and the j^{th} measured diffraction pattern). In Fig. 4, it is found that the "correct" distance $z = z_0$ does not coincide with a minimum of R, indicating that its value cannot be used to discard solutions which are incorrect. An alternative approach that is resistant to errors in z (for errors up to 20%), and can produce reconstructions with the correct number of spokes is an image cross-correlation based method for position determination [6].

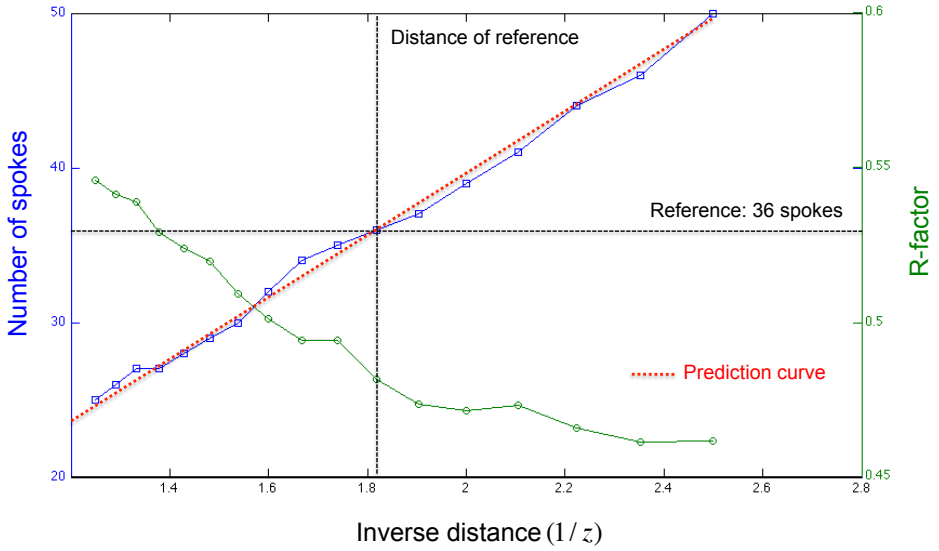

Fig. 4. Number of spokes as a function of the assumed sample-to-camera distance z in the range 0.4 m to 0.8 m. The distance of reference, where the measured data were taken, is $z_0 = 0.55\,\mathrm{m}$ ($\approx 1.8\,\mathrm{m}^{-1}$ in this plot) and the number of spokes for the reference object is 36. The red dotted line is the predicted number of spokes (see discussion). For each z value used, the corresponding R-factor is plotted (calculated at iteration 100 with all 460 frames).

4.1. Numerical simulations

To understand the experimental results seen in section 4, simulations of the experiment were performed with conditions as close as possible to the experimental ones. The number of spokes produced in these simulations reproduced the curve shown Fig. 4. In common with the experimental reconstructions, the phase reconstructions in the simulations are clearer and cleaner than

the amplitude reconstructions, as shown in Fig. 5, where the use of $z = 0.5$ m has produced a reconstruction with 39 spokes. To distinguish the possibility that the choice of algorithm was not responsible for the observed effect, separate reconstructions using DM and ePIE [4] algorithms were carried out, with each showing same behaviour.

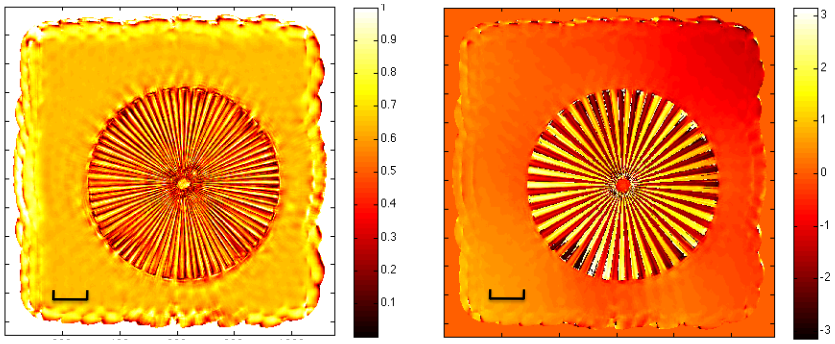

Fig. 5. Amplitude and phase of a reconstructed Siemens star at 0.5 m, showing 39 spokes. These results from a numerical simulation can be compared directly with the reconstruction based on experimental measurements that is shown in Figure 3(b). Scale bar, 2 μm.

In CDI the correct size of the support is empirically known to eliminate the incorrect solution, and changing the distance parameter z in ptychography has a similar effect to changing the size of the support in CDI, suggesting that the results in Fig. 3 could resemble out-of-focus images, and that the change in the spoke number with distance parameter z could be similar to the Talbot effect for linear gratings [21, 22]. The Talbot effect is a self-imaging phenomenon in which there are periodic variations in the Fresnel diffraction pattern along the direction of propagation, with the original grating pattern reappearing at integer multiples of the Talbot length, and a variety of patterns with smaller periods appearing at fractions of the Talbot length. The Fresnel diffraction pattern at distance z from an object O can be calculated using a Fresnel propagator in Fourier space given by

$$O(z) = \mathscr{F}^{-1}[\exp(\frac{-izq^2}{2k})\mathscr{F}(O)] \tag{3}$$

where $\mathscr{F}$ denotes a Fourier transform operation, and the wavenumber $k = 2\pi/\lambda$. Using this approach, simulated images of Siemens stars were propagated to distances which should produce extra spokes, but the resulting spoke patterns were found to be rather different, as shown in Fig. 6, so the different reconstructions shown in Fig. 3 are not related simply by Fresnel propagation.

Another concern was that direct-space objects with a high degree of circular symmetry, combined with a circular scan, would produce the observed pathology. The circular scan was originally suggested for the purpose of eliminating grid artefacts in ptychography [18] and was found to improve data convergence and to reduce ambiguities in data reconstructions by breaking the translation symmetries. Therefore, raster scans based on a square grid were compared to circular scans. In practice both type of scan showed the same pathology as in Fig. 3 so this behaviour is independent of the scan mode. Thinner Siemens stars, that imparted smaller phase shifts $(\pi/2, \pi/3)$ to the x-ray beam, were also simulated to test whether the results could be attributed to phase wraps coming from helical phase ramps, but the response in the images was the same as reported in Fig. 4.

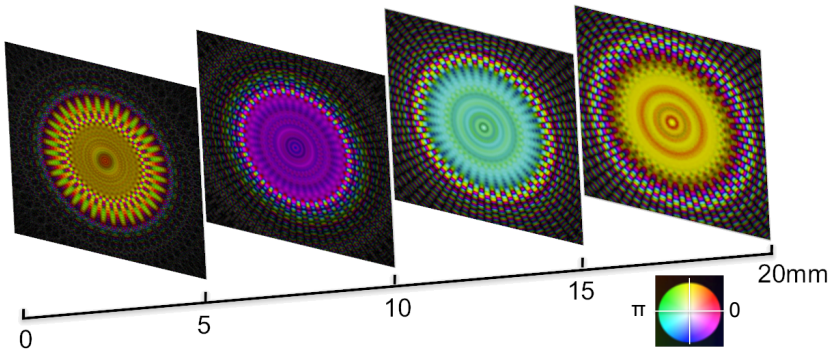

Fig. 6. Computed free-space propagation of the simulated Siemens star to planes situated at 5 mm intervals upstream from the reference position. The colour rendering shows complex valued data after histogram equalisation to stretch the contrast of the images.

5. Discussions and conclusions

We have seen in section 3 that probes with increased divergence show higher quality reconstructions despite a reduced degree of overlap. This indicates that probe bandwidth and probe overlap are complementary factors, while the sampling of the probe is another important factor, particularly when an increasing fraction of the signal power lies within the CDI window as the camera length z is increased.

An unexpected pathology was discovered in the images of a symmetric star-shaped object: images were found to show the wrong number of spokes. Fig. 3 shows clearly that the size of the stars is the same when measured in units of the scanner (closed scale bars) but not when the scale is set by the size of the CDI window (open scale bars). The spacing of the spokes varies in the opposite way: the spokes have a period which is constant in units of the CDI window size (open scale bars). Spokes with a real spacing d produce features on the detector with a separation of $\lambda z_0/d$, so if an incorrect detector distance z is used in the reconstruction process, the spacing of the reconstructed spokes is wrong by a factor z_0/z. The conflict between the length scales results in a different number of spokes for star patterns reconstructed with the detector located at $z \neq z_0$, as plotted in Fig. 4, where there is good agreement between the observations and the predictions of the model.

Our numerical simulations have reproduced the experimental results and we have shown that a non-unique reconstruction can be found for symmetric objects in ptychography if the scan parameters are not accurately known.

A question that needs to be addressed is whether the benefits of having more probe structure in the CDI window at the cost of coherence (by adjusting slit openings beyond the nominal coherence length) is better than having less structure with a higher degree of coherence, since the partial coherence can, in principle, be corrected for during post-processing of the recorded data [23].

Acknowledgements

Use of the Advanced Photon Source, an Office of Science User Facility operated for the U.S. Department of Energy (DOE) Office of Science by Argonne National Laboratory, was supported by the U.S. DOE under Contract No. DE-AC02-06CH11357. Beamline 34-ID-C was built with a grant from the National Science Foundation DMR-9724294. This research was

carried out under grants EP/G 068437/1 and EP/ I 022562/1 from the UK Engineering and Physical Sciences Research Council (EPSRC).